Available online at www.sciencedirect.com
ScienceDirect
Journal of Sound and Vibration 318 (2008) 792–808
JOURNAL OF SOUND AND VIBRATION
www.elsevier.com/locate/jsvi

Realization of a broadband low-frequency plate silencer using sandwich plates

Chunqi Wang[a], Li Cheng[a,*], Lixi Huang[b]

[a]*Department of Mechanical Engineering, The Hong Kong Polytechnic University, Kowloon, Hong Kong*
[b]*Department of Mechanical Engineering, The University of Hong Kong, Pokfulam Road, Hong Kong*

Received 17 September 2007; received in revised form 25 February 2008; accepted 27 April 2008
Handling Editor: L.G. Tham
Available online 20 June 2008

Abstract

A broadband low-frequency plate silencer is realized experimentally using sandwich plates. The silencer consists of an expansion chamber with two side-branch cavities, each covered by a light but extremely stiff plate. The requirement for high bending stiffness and low density of the plate is satisfied with a sandwich construction by adhering two high-rigidity thin sheets with a relatively thick and light foam core. A test rig is built with a square duct of 100 mm in dimension, and each cavity is 100 mm deep and 500 mm long. Three types of sandwich plates with different mechanical properties are tested. The plate having the highest bending stiffness and lowest density results in a measured stopband from 133 to 274 Hz in which the transmission loss is higher than 10 dB over the whole frequency band. Comparisons between the three sandwich plates partly confirm the theoretical findings on the effect of plate properties on the silencer performance. It is also shown that the mathematical model based on homogeneous plates can provide satisfactory prediction on the performance of a sandwich plate silencer in the low-frequency range of interest. Experimental and theoretical results are found to be in fair agreement.

1. Introduction

Low-frequency duct noise is difficult to deal with by passive methods and remains a technical challenge. Lining a duct with porous sound absorbing material is a mature and reliable technique that can tackle the medium-to-high-frequency noise [1,2]. However, it does not work well at very low frequencies. An expansion chamber-type muffler may be used to reduce the low-frequency noise, but such a device is usually bulky and pressure loss exists. It is well known that one detrimental effect associated with the expansion chamber-type muffler is the back pressure due to the discontinuity of the duct cross-section. The back pressure results in extra power consumption; hence, more noise could be generated by the additional power required to overcome the pressure loss. To reduce the back pressure, straight-through concentric resonator, plug muffler, and three-duct cross-flow muffler have been proposed and their performance has been experimentally assessed [3]. These designs can reduce but cannot eliminate the back pressure. For the purpose of a broadband passive noise

*Corresponding author.
E-mail address: mmlcheng@polyu.edu.hk (L. Cheng).

0022-460X/$ - see front matter © 2008 Elsevier Ltd. All rights reserved.
doi:10.1016/j.jsv.2008.04.054

control device, which works effectively in the low- to medium-frequency range, Huang [4] proposed the concept of drumlike silencer, which consists of an expansion chamber with two side-branch cavities covered by light membranes under high tension. The predicted broadband noise reflection by the drumlike silencer has been verified without and with flow [5,6]. When compared with porous duct lining and expansion chamber, the drumlike silencer carries the extra merits of being environmentally friendly and creating zero pressure loss. Previous studies showed that the tension applied on the membranes plays an important role in achieving the desired performance [4,5]. In practice, however, it is not easy to tune and to maintain the tension at the expected value, since the tension may vary due to membrane relaxation or the change of ambient temperature.

In a recent theoretical study, Huang [7] replaced the membrane used in the drumlike silencer described above by a simply supported plate, hence a plate silencer. As the plate uses its natural bending moment as the sole structural restoring force, problems related to tension maintaining are avoided. Additionally, theoretical study showed that the proposed plate silencer may achieve a much wider logarithmic bandwidth than the drumlike silencer of the same cavity geometry due to the change in the intermodal acoustic interference between the odd and even *in vacuo* vibration modes [7]. Due to the apparent difficulty in implementing the simply supported boundary condition in an acoustic system like the plate silencer, Wang et al. [8] extended the theoretical study to plates with both the leading and trailing edges clamped, and tested the idea using balsawood plates experimentally. According to the theoretical studies, a good plate silencer requires very light but extremely stiff plates, irrespective of the plate boundaries [7,8]. Such a condition is generally difficult to satisfy with existing homogeneous plate. Although the balsawood used in Ref. [8] is one of the best materials for this purpose according to chart 1 given in Ref. [9], it is still too heavy and soft for the plate silencer. Hence, the prototype device in Ref. [8] only works in a relatively narrow frequency range with the overall stopband shifted to higher frequencies.

As a continuation of our previous work, this study aims to realize a broadband low-frequency plate silencer using sandwich construction. The sandwich plate combines high bending stiffness with low weight, making it a preferable choice for the design of plate silencer. However, the sandwich construction also makes it difficult to model the coupling dynamics between the plate vibration and the acoustics. Therefore, the following two tasks are performed in the present work. First, the possibility is explored of representing the sandwich plate with an Euler–Bernoulli beam in the two-dimensional (2D) plate silencer modelling, and a simplified mathematical model is then established for the sandwich plate silencer, which is shown to be a useful simulation tool to guide the practical design of the silencer. Second, design considerations for the plate silencer are discussed based on the 2D model, and three sandwich plate silencers are prototyped and tested experimentally. Experimental results are analyzed and compared with theoretical predictions.

2. Theoretical outline

Fig. 1 shows the 2D configuration of a side-branch plate silencer. A rectangular duct is modelled by a 2D channel of height h^*, with two plates (beams, in the 2D model) flush mounted on the rigid duct walls. The plates are clamped at the edges $|x^*| = L^*/2$, each backed by a rigid-walled cavity of depth h_c^*. The other lateral edges of the plates are set free so that the plates can respond to incident waves with high vibration magnitude. When a sound wave is incident from the left-hand side of the duct, it induces the plates to vibrate and the vibration radiates sound waves towards both ends of the duct. The left-going waves form the reflected sound, while the right-going waves combine with the incident wave to form the transmitted sound. The principle of acoustic energy conservation guarantees that, whatever amount of sound reflection is, the same amount of reduction is induced in the sound energy flux transmitted to the downstream of the duct. In other words, it is assumed that the performance of the plate silencer is dominated by the sound reflection due to the plate vibration.

In the following presentation, all parameters are normalized by three basic quantities: air density, ρ_0^*, speed of sound, c_0^*, and the duct height, h^*. The normalization schemes for some typical parameters are given below:

$$\begin{aligned} &x = \frac{x^*}{h^*}, \quad y = \frac{y^*}{h^*}, \ \eta = \frac{\eta^*}{h^*}, \quad L = \frac{L^*}{h^*}, \ h_c = \frac{h_c^*}{h^*}, \quad k_0 = \frac{\omega^* h^*}{c_0^*}, \ t = \frac{c_0^* t^*}{h^*}, \\ &f = \frac{f^* h^*}{c_0^*}, \ \omega = 2\pi f = k_0, \quad p = \frac{p^*}{\rho_0^*(c_0^*)^2}, \ B = \frac{B^*}{(h^*)^3 \rho_0^*(c_0^*)^2}, \quad m = \frac{m_s^*}{\rho_0^* h^*}, \end{aligned} \tag{1}$$

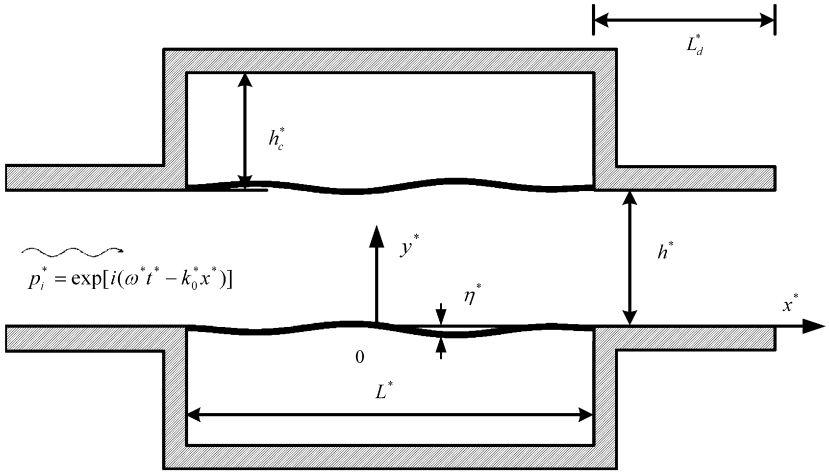

Fig. 1. Two-dimensional theoretical model for a clamped plate silencer.

where f is the dimensionless frequency, p is the dimensionless acoustic pressure, B is the dimensionless bending stiffness. With m_s^* being the surface density of the plate, m can be called the plate-to-air mass ratio, or just the mass ratio. To avoid confusion, the dimensional parameters are always denoted by asterisks while the corresponding dimensionless ones are not.

2.1. Theoretical modelling

In order to calculate the silencing performance of the plate silencer, the coupled dynamics problem of the plates is solved. Suppose that a plane incident wave comes from the left-hand side of the duct with unit amplitude

$$p_i = \exp[\mathrm{i}(\omega t - k_0 x)], \tag{2}$$

and it causes the plate to vibrate with a transverse displacement $\eta(x,t)$. For a homogeneous plate with bending stiffness, B, and mass ratio, m, the vibration of the lower plate is governed by the following equation:

$$B(1 + \mathrm{i}\sigma_s)\frac{\partial^4 \eta}{\partial x^4} + m(1 - \mathrm{i}\sigma_m)\frac{\partial^2 \eta}{\partial t^2} + (p_i + \Delta p) = 0, \tag{3}$$

where p_i is the dimensionless incident wave; $\Delta p = p_+ - p_-$ is the fluid loading acting on the duct side (+) and cavity side (−) of the plate induced by the plate vibration itself; σ_m and σ_s are the mass and stiffness damping coefficients for the Rayleigh damping model adopted to account for the structural damping in the plate. Generally, it is appropriate to represent a thin plate of homogeneous material with an Euler–Bernoulli beam in a 2D model as shown in Eq. (3). For such an ideal model, deflection of the beam is caused by bending only, and there is no shear effect involved. However, for a sandwich plate to be investigated in this study, its deflection is caused not only by bending but also by shear and rotation in the core [10]. Hence, strictly speaking, the coupled dynamic equation for a sandwich plate is different from Eq. (3) that is based on a homogeneous plate. However, for the plate silencer design, the sandwich plate functions in a very low-frequency range. In this frequency range, the flexural motion of a sandwich beam is mainly determined by pure bending [11], so that the shear effects can be neglected. As a result, it is argued that it is reasonable to predict the performance of a sandwich plate silencer with a model based on homogeneous plate. In other words, the sandwich plate may be treated as homogeneous in the plate silencer design. This argument is validated in the following experimental study.

For a harmonic vibration with angular frequency ω, the normal velocity of the plate is related to the transverse displacement as

$$V(x,t) = \frac{\partial \eta(x,t)}{\partial t} = \mathrm{i}\omega\eta(x,t). \tag{4}$$

Then dynamic Equation (3) is transformed as

$$(1+\mathrm{i}\sigma_s)\frac{B}{i\omega}\frac{\partial^4 V}{\partial x^4}+\mathrm{i}\omega m(1-\mathrm{i}\sigma_m)V+(p_i+\Delta p)=0. \tag{5}$$

Note that the incident sound wave p_i, the transverse displacement $\eta(x,t)$ and the normal velocity $V(x,t)$ are with the same time dependence $\exp(\mathrm{i}\omega t)$, which is henceforth omitted.

Following the Galerkin procedure, the plate vibration velocity, $V(x)$, is expanded as a series of *in vacuo* modes, $\varphi_j(\xi)$, of a clamped uniform Euler–Bernoulli beam with modal amplitudes V_j:

$$V(x)=\sum_{j=1}^{\infty}V_j\varphi_j(\xi), \tag{6}$$

$$V_j=\int_0^1 V\varphi_j(\xi)\,\mathrm{d}\xi,\ \xi=x/L+1/2. \tag{7}$$

The vibration mode shapes, $\varphi_j(\xi)$, are given as [12]

$$\varphi_j(\xi)=A_{1,j}\mathrm{e}^{\beta_j\xi}+A_{2,j}\mathrm{e}^{-\beta_j\xi}+A_{3,j}\sin(\beta_j\xi)+A_{4,j}\cos(\beta_j\xi) \tag{8}$$

with

$$\begin{gathered}A_{1,j}=\tfrac{1}{2}(1-\sigma_j),\ A_{2,j}=\tfrac{1}{2}(1+\sigma_j),\ A_{3,j}=\sigma_j,\ A_{4,j}=-1,\\ \sigma_j=\frac{\cosh(\beta_j)-\cos(\beta_j)}{\sinh(\beta_j)-\sin(\beta_j)},\ \cos(\beta_j)\cosh(\beta_j)=1.\end{gathered} \tag{9}$$

In order to solve Eq. (5), the fluid loading Δp is related to the modal vibration velocity amplitude V_j through a modal impedance matrix $\{Z_{jl}\}$ as shown below [8]:

$$\Delta p=\sum_{l=1}^{\infty}\left(\sum_{j=1}^{\infty}V_jZ_{jl}\right)\varphi_l(\xi) \tag{10}$$

with Z_{jl} defined as

$$Z_{jl}=\int_0^1\varphi_l(\xi)\Delta p_j(x)\,\mathrm{d}\xi, \tag{11}$$

where $\Delta p_j(x)$ is the fluid loading caused by the jth modal vibration of unit amplitude. As $V(x)$ is expanded as a series of *in vacuo* modes in Eq. (6), the sum in parentheses in Eq. (10) takes into account the response of all vibration modes.

Details of finding the modal impedance Z_{jl} can be found in Ref. [8]. Here, only a brief description of the procedure is given. To begin with, the fluid loading induced by the plate vibration, Δp, is divided into two parts:

$$\Delta p=p_{+\mathrm{rad}}-p_{\mathrm{cav}}, \tag{12}$$

where $p_{+\mathrm{rad}}$ is the radiation sound pressure in the main duct, and p_{cav} is the pressure inside the cavity acting on the lower plate surface. The formulation for $p_{+\mathrm{rad}}$ is known as [13]

$$p_{+\mathrm{rad}}(x,y)=\frac{L}{2}\sum_{n=0}^{\infty}c_n\psi_n(y)\int_0^1\psi_n(y')V(x')\times[H(x-x')\mathrm{e}^{-\mathrm{i}k_n(x-x')}+H(x'-x)\mathrm{e}^{+\mathrm{i}k_n(x-x')}]\,\mathrm{d}\xi', \tag{13}$$

where $y'=0$ denotes the y coordinate of the lower plate surface, H is the Heaviside function, c_n, k_n, and ψ_n are, respectively, the modal phase speed, the modal wave number, and the modal velocity potential:

$$c_n=\frac{\mathrm{i}}{\sqrt{(n\pi/\omega)^2-1}},\ k_n=\frac{\omega}{c_n},\quad \psi_n(y)=\sqrt{2-\delta_{0n}}\cos(n\pi y), \tag{14}$$

and δ_{0n} is the Kronecker delta. Hence, assuming that the radiation pressure caused by the jth modal vibration of unit amplitude φ_j is $p_{+\mathrm{rad},j}$, the modal impedance contributed by the radiation pressure in the main duct is found as

$$Z_{+jl} = \int_0^1 \varphi_l(\xi) p_{+\mathrm{rad},j}(x,0)\,\mathrm{d}\xi. \tag{15}$$

The acoustic pressure inside the cavity, p_{cav}, can be expressed in terms of "rigid wall" modes of the cavity [14]:

$$p_{\mathrm{cav}}(x,y) = \sum_{m,n} \frac{-\mathrm{i}\omega\phi_{m,n}(x,y)}{Lh_c(\kappa_{m,n}^2 - k_0^2 + 2\mathrm{i}\zeta_{m,n}\kappa_{m,n}k_0)} \int_0^1 V(x',0)\phi_{m,n}(x',0)\,\mathrm{d}\xi', \tag{16}$$

where $V(x',0)$ is the normal velocity over the vibrating plate, $\zeta_{m,n}$ is the damping ratio of the (m,n)th acoustic mode $\phi_{m,n}(x,y)$, L is the length of the cavity, h_c is the depth of the cavity, and $\kappa_{m,n}$ is the corresponding acoustic wave-number of the (m,n)th acoustic mode $\phi_{m,n}(x,y)$, with $\phi_{m,n}(x,y)$ and $\kappa_{m,n}$ given as

$$\phi_{m,n}(x,y) = \sqrt{(2-\delta_{0m})(2-\delta_{0n})}\cos\left(\frac{m\pi x}{L}\right)\cos\left(\frac{n\pi y}{h_c}\right), \tag{17}$$

$$\kappa_{m,n}^2 = \left(\frac{m\pi}{L}\right)^2 + \left(\frac{n\pi}{h_c}\right)^2. \tag{18}$$

Therefore, the cavity pressure caused by the jth modal vibration of unit amplitude, $p_{\mathrm{cav},j}(x,y)$, can be found and the cavity modal impedance contributed by the pressure inside the cavity is given as

$$Z_{\mathrm{cav},jl} = -\int_0^1 \varphi_l(\xi) p_{\mathrm{cav},j}(x,0)\,\mathrm{d}\xi. \tag{19}$$

With the modal impedances due to $p_{+\mathrm{rad}}$ and p_{cav} found in Eqs. (15) and (19), the total modal impedance defined in Eq. (11) is given as

$$Z_{jl} = Z_{+jl} + Z_{\mathrm{cav},jl}. \tag{20}$$

To solve the coupled dynamics problem described above, Eq. (6) is first substituted into Eq. (5). The resulting equation is then multiplied by $\varphi_j(\xi)$ and integrated over the beam surface. Making use of the orthogonality property of the mode shape $\varphi_j(\xi)$, Eq. (5) becomes a truncated set of linear equations:

$$\begin{bmatrix} Z_{11}+L_1 & Z_{12} & \cdots & Z_{1N} \\ Z_{21} & Z_{22}+L_2 & \cdots & Z_{2N} \\ \cdots & \cdots & \cdots & \cdots \\ Z_{N1} & Z_{N2} & \cdots & Z_{NN}+L_N \end{bmatrix} \begin{Bmatrix} V_1 \\ V_2 \\ \vdots \\ V_N \end{Bmatrix} + \begin{Bmatrix} I_1 \\ I_2 \\ \vdots \\ I_N \end{Bmatrix} = 0, \tag{21}$$

where I_j is the modal coefficient of the incident wave, and L_j is mainly determined by the plate property

$$I_j = \int_0^1 p_i \varphi_j(\xi)\,\mathrm{d}\xi, \tag{22}$$

$$L_j = (1-\mathrm{i}\sigma_m)m\mathrm{i}\omega + (1+\mathrm{i}\sigma_s)\frac{B}{\mathrm{i}\omega}\left(\frac{\beta_j}{L}\right)^4. \tag{23}$$

Eq. (21) can be solved via the inversion of matrix, and the vibration velocity is found by substituting the modal vibration coefficient V_j into Eq. (6).

The total sound pressure transmitted to the downstream, p_t, is found by adding the incident wave, p_i, to the far-field radiation wave, $p_{+\mathrm{rad}}$, which can be found from Eq. (13) by taking only the plane wave mode $n=0$ for $x > L/2$. Similarly, the reflected wave, p_r, is found from Eq. (13) by taking only the plane wave mode $n=0$ for $x < L/2$. Hence, the sound reflection coefficient, β, absorption coefficient (if any), α, and the transmission

loss (TL) are evaluated as follows:

$$p_t = p_{+\mathrm{rad}}|_{n=0,x\to+\infty} + p_i, \quad p_r = p_{+\mathrm{rad}}|_{n=0,x\to-\infty},$$
$$\beta = \left|\frac{p_r}{p_i}\right|^2, \quad \alpha = 1-\beta-\left|\frac{p_t}{p_i}\right|^2, \quad \mathrm{TL} = 20\log_{10}\frac{|p_i|}{|p_t|}. \tag{24}$$

The complex amplitude of the reflected sound, p_r, is the sum of the contributions made by all individual plate vibration modes, which is shown as

$$p_r = \frac{1}{2}\int_{-L/2}^{+L/2} V(x')\mathrm{e}^{-\mathrm{i}k_0x'}\mathrm{d}x' = \sum_{j=0}^{N} V_jR_j$$

with

$$R_j = \int_{-L/2}^{+L/2} \varphi_j(\xi')\mathrm{e}^{-\mathrm{i}k_0x'}\mathrm{d}x', \tag{25}$$

where R_j is the complex amplitude of the reflected sound by the induced vibration of the jth mode with unit amplitude.

2.2. Discussion

In actual calculations, modal truncation is necessary for both the vibration modes and the acoustic modes [8,15]. For the plate vibration, up to 25 vibration modes are used. Numerical results show that the number of modes is normally enough as further increase in the number does not make significant difference for the purpose of this study. Although higher modes are used in the above modelling, only the lowest few modes contribute significantly to the reflected sound, as demonstrated in the following numerical example. Fig. 2 shows the performance of a typical side-branch plate silencer with the following parameters:

$$L = 5,\ h_c = 1, \quad m = 2.4,\ B = 0.11, \quad \sigma_m = \sigma_s = 0. \tag{26}$$

Fig. 2(a) shows the overall TL spectrum. Fig. 2(b–e) shows the amplitudes of the single-mode reflection, $|V_jR_j|$, by the first four *in vacuo* vibration modes. It is clear that the first and second modes dominate the sound reflection in the frequency range of interest. Actually, as the order of the vibration mode increases, both the modal vibration coefficients, V_j, and the mode reflection, $|V_jR_j|$, decrease quickly.

Note that there are considerations of the validity of the 2D model in dealing with the actual silencer design. In the current study, the cross-section of the duct is assumed to be square or rectangular. The leading and trailing edges of the plate are fixed while the other two lateral edges are set to move freely. When the frequency is below the first cut-on frequency of the duct, that is $f<0.5$, the incident sound wave consists of plane wave only. For plates within typical large length/width ratios considered in this paper, it is unlikely that unevenness of the plate motion and that of radiated pressure along lateral direction plays a significant role. This problem has been investigated in Ref. [15] for a drumlike silencer which uses a tensioned membrane instead of the plate. For frequencies higher than the first cut-on frequency of the duct, three-dimensional (3D) effect may occur and the 2D model may become questionable. However, since the plate silencer mainly targets the low-frequency noise, the physical model is accurate enough as long as the frequency of interest is below the first cut-on frequency.

3. Design of the plate silencer

Aiming for a broadband plate silencer that works preferably in the low-frequency range, the following three issues are addressed at the design stage. First, the effect of various design parameters on the performance of the plate silencer should be identified. Although the plate silencer can be a very simple device for construction, it does have a lot of design variables, for instance, the cavity shape, the plate-to-air mass ratio, the bending stiffness, the structural damping in the plate as well as the sound energy damping in the cavity and duct [7,8,16]. In this section, some main points about these design parameters are summarized to use as guidelines

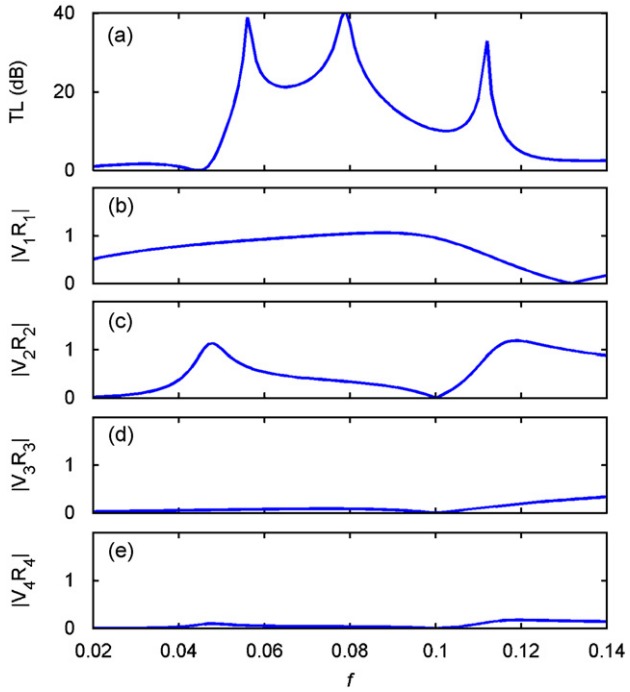

Fig. 2. Amplitudes of the single-mode reflection, $|V_jR_j|$, by the first four *in vacuo* vibration modes of a typical clamped plate silencer with $L = 5$, $h_c = 1$, $m = 2.4$, and $B = 0.11$. (a) TL. (b)–(e): $|V_1R_1|$–$|V_4R_4|$.

for the plate silencer design. The second issue is on the performance parameter of the silencer. As TL is independent of the source and terminations at the downstream end, it is easy to predict, and hence it is chosen as the performance parameter. However, the terminal reflection cannot be neglected in the real application of finite duct length. In order to examine the influence of terminal conditions, it is necessary to evaluate the insertion loss (IL) of the plate silencer for a finite duct. Finally, the feasibility of using sandwich construction to fulfill the requirement for plate properties is investigated theoretically, and three types of sandwich plates with different mass ratios and bending stiffnesses are manufactured.

3.1. Cavity shape

The hard-walled cavity serves to prevent the break-out noise. Meanwhile it also introduces cavity air stiffness to the system which may reduce the effectiveness of the plate silencer, especially at low frequencies. Aiming for the widest stopband with a given volume of $\Lambda = Lh_c$, an optimization study of the cavity parameters has been carried out for the drumlike silencer [16]. Because of the similarity of configurations between the drumlike silencer and the plate silencer, most of the findings in Ref. [16] also apply to the design of a plate silencer. Briefly, for given cavity volume, shallower cavity with longer plate has wider TL spectrum. The frequency interval between spectral peaks increases and, as a result, the dip between adjacent peaks falls down. On the other hand, deeper and shorter cavity works in a narrower frequency band with better minimal TL. For a simply supported plate silencer, the optimal cavity shape for the specific volume of $Lh_c = 5h^2$ was found to be $L_{\text{opt}} = 5h$ [7]. This configuration is taken as the default in the current study.

3.2. Plate properties

The plate-to-air mass ratio, m, and the bending stiffness, B, are two crucial parameters that affect the silencing performance of the silencer significantly. The effect of plate mass is generally counterproductive. As the mass ratio m increases, the maximum achievable bandwidth decreases, while the lower band limit and the

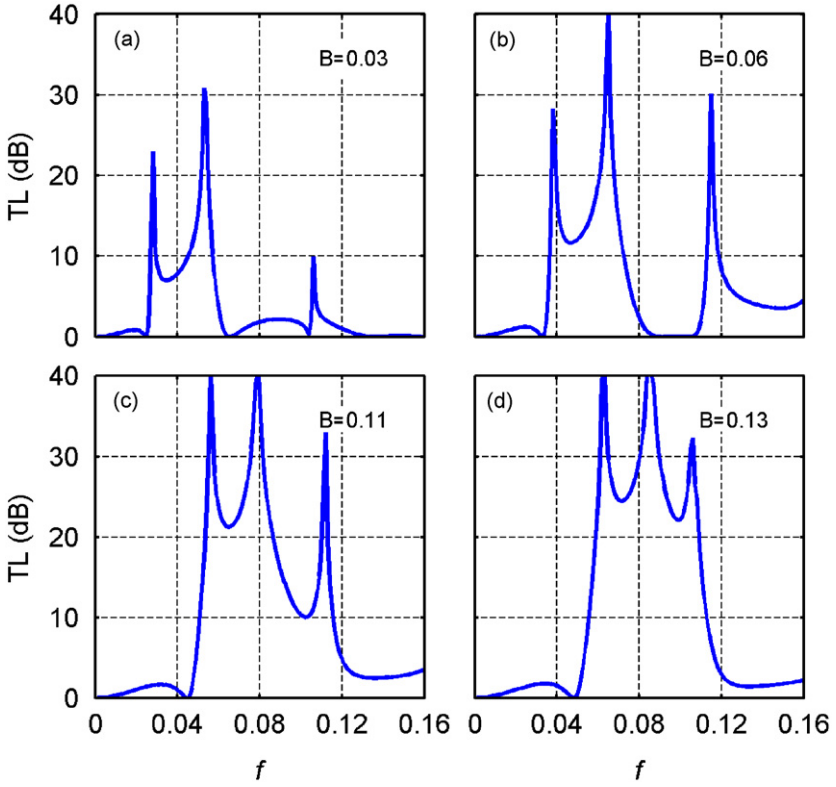

Fig. 3. Variation of TL spectrum with respect to the bending stiffness, B, for a clamped plate silencer with $L = 5$, $h_c = 1$ and $m = 2.4$.

required bending stiffness increase, as reported in the earlier theoretical study [8]. The bending stiffness, B, plays a delicate role in the sound reflection of the plate silencer. Fig. 3 shows the variation of TL spectrum with respect to four different values of B. The mass ratio is fixed at $m = 2.4$, and the cavity geometry is $L = 5$ and $h_c = 1$. Three spectral peaks can be observed for all the four cases in the frequency range of interest. However, when the bending stiffness is insufficient, dips between the spectral peaks are so pronounced that the silencer works effectively only at the discrete resonant frequencies, as shown in Fig. 3(a). As the bending stiffness increases, the spectral peaks shift towards higher frequencies, as demonstrated in Fig. 3(b) and (c). At the same time, the trough between the first and second spectral peaks is first lifted up and then the trough between the second and third peaks, which warrants good performance of the silencer over a broad frequency range instead of only at the spectral peaks. Generally speaking, a three-peak stopband shown in Fig. 3(c) is wider than a two-peak stopband in Fig. 3(b). However, since the low-frequency noise (say, $f<0.077$) is of the most interest, the two-peak stopband spectrum shown in Fig. 3(b) may also be chosen as a practical silencer design. Higher bending stiffness may further increase the TL between the spectral peaks, but, as a compromise, the whole spectrum shifts towards higher frequencies and the bandwidth shrinks, as shown in Fig. 3(d).

3.3. Comparison between TL and IL

In this study, the silencing performance of the plate silencer is characterized by a wide stopband, $f \in [f_1, f_2]$, in which the TL is above a criterion value, TL_{cr}, over the whole frequency range. As recommended in Ref. [16], the criterion value may be chosen as the peak TL for an expansion chamber whose cavity volume is three times the actual cavity volume in the plate silencer. For a plate silencer with two cavities of depth h, TL_{cr} can be calculated and rounded up to 10 dB. However, as the duct is usually finite in the real application, the no-reflection termination in the TL calculation cannot always be satisfied, and the terminal reflection may influence the performance of the plate silencer more or less. In this situation, the IL, which shows the

difference between the acoustic power radiated without any silencer and that with the silencer, is needed to assess the performance of the plate silencer.

The IL of the plate silencer specified in Eq. (26) is calculated to address the difference between the TL and the IL in the plate silencer design. Besides the configuration of the plate silencer itself, it requires the prior knowledge of the internal impedance of the sound source and the termination conditions to predict the IL. For a finite circular duct of radius r without any flange at the downstream termination, the open-end impedance at very low frequencies can be described by [17]

$$Z_r = \frac{(k_0 r)^2}{4} + \mathrm{i}0.6k_0 r. \tag{27}$$

The open-end impedance of the square duct is assumed equal to that of a circular duct with the same cross-section areas. If an independent sound source with constant amplitude of incident wave is assumed, the IL of the plate silencer can be calculated as [18]

$$\mathrm{IL} = 20\log_{10}\left|\left\{\mathrm{e}^{-\mathrm{i}k_\alpha L_d}(1+R)\Big/\left[p_t\mathrm{e}^{-\mathrm{i}k_\alpha L_d} + \frac{p_t\mathrm{e}^{-\mathrm{i}k_\alpha L_d}R(p_r\mathrm{e}^{-\mathrm{i}k_\alpha L_d} + \mathrm{e}^{\mathrm{i}k_\alpha L_d})}{\mathrm{e}^{\mathrm{i}k_\alpha L_d} - p_r\mathrm{e}^{-\mathrm{i}k_\alpha L_d}R}\right]\right\}\right|, \tag{28}$$

where $R = (Z_r - 1)/(Z_r + 1)$, L_d is the distance from the expansion chamber exit to the downstream end as shown in Fig. 1, and the complex wavenumber k_α is defined as

$$k_\alpha = k_0 + (1 - \mathrm{i})\alpha_{\mathrm{wall}}, \tag{29}$$

where α_{wall} is the attenuation coefficient due to the viscous effect within the interior of the duct [19]. Fig. 4 compares the TL and the IL of the plate silencers specified in Eq. (26) for $L_d = 1h$, $3h$, $9h$, and $500h$. For short ducts with $L_d = 1h$, $3h$, $9h$, the terminal reflection due to the open-end impedance does influence the performance of the silencer obviously, and the corresponding IL spectra vary with the distance, L_d, as shown in Fig. 4(a)–(c). Since IL better represents the performance of the noise reduction device in real use, the silencer should be tuned to IL optimization (for example, by adjusting L_d) instead of TL optimization wherever the termination condition is known. When compared with the TL spectrum, however, both sets of results show similar variations especially in terms of peak locations. If the TL is high at some frequencies, the IL will also be high in general. As viscous damping is applied to the duct, a longer L_d tends to diminish the effect of the terminal reflection, which leads to a rapprochement between TL and IL as shown in Fig. 4(d). We can therefore summarize by saying that it is appropriate to use TL to describe the performance of the plate silencer for the sake of simplicity it offers, although there are slight differences between the IL and the TL spectra.

Note that negative IL is found at frequencies for which the transmitted wave is enhanced by multiple reflections at the end termination and the silencer. This phenomenon is common to all reactive silencers. For the present configuration, the silencer is equivalent to a pressure release device at frequencies where the silencer is effective. As the open end is also approximately a pressure-release point, downstream resonance occurs whenever the downstream distance length L_d (plus a certain distance into the silencer) approaches half a wavelength. When the downstream distance is very short, such resonance occurs at high frequencies and is of little concern for the design of current low-frequency silencer. This trend of high frequency for $\mathrm{IL} < 0$ for short downstream length is shown in Fig. 5. Having said these, it is emphasized that there is no significant overall difference between the TL and IL curves, and it suffices to aim at high TL for a broad frequency band.

3.4. Construction of the sandwich plate

The sandwich plate consists of two thin aluminium sheets each of thickness h_t, separated by a thick core of thickness h_0, as shown in Fig. 6(a). The Young's modulus E_t and density ρ_t for the aluminium sheet are 4.87×10^5 (69 GPa) and 2204 (2700 kg/m^3), respectively. The values shown in the brackets are the corresponding dimensional values, which are calculated with air density $\rho_0^* = 1.225\,\mathrm{kg/m^3}$ and speed of sound $c_0^* = 340\,\mathrm{m/s}$. The core material is Rohacell® IG-31 [20] with the density, ρ_{Rohacell}, and Young's modulus, E_{Rohacell} being 26 (32 kg/m^3) and 254 (36 MPa), respectively. For such a three-layer sandwich construction, the effective bending stiffness per unit width of the beam is found as [21]

$$B = \tfrac{1}{6}E_t h_t^3 + \tfrac{1}{2}E_t h_t(h_t + h_0)^2 + \tfrac{1}{12}E_{\mathrm{Rohacell}}h_0^3. \tag{30}$$

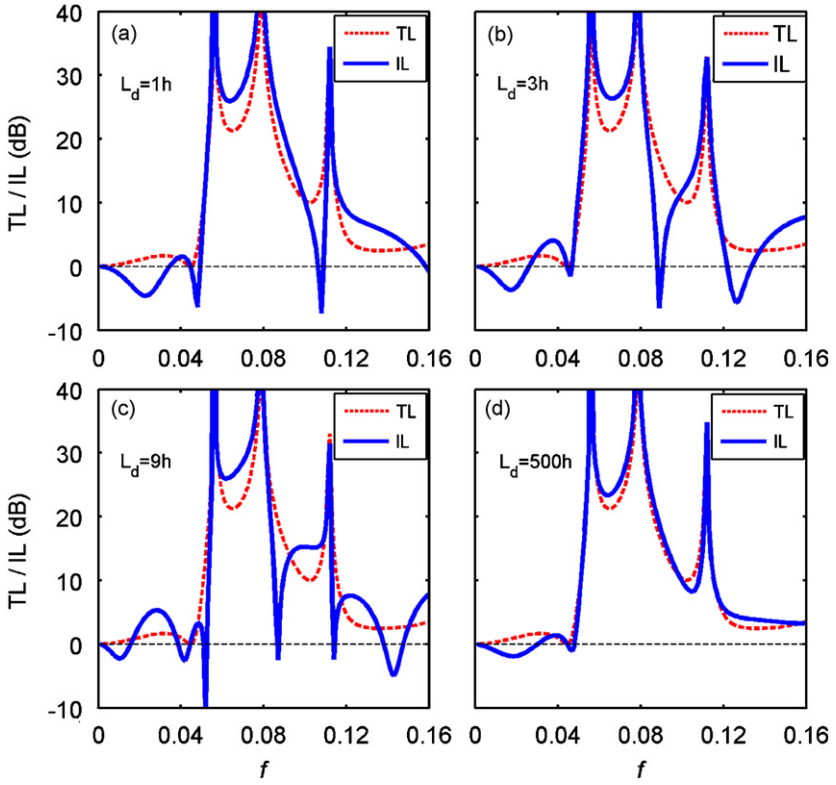

Fig. 4. Comparison between TL and IL of a clamped plate silencer with $L = 5$, $h_c = 1$, $m = 2.4$, $B = 0.11$ and $L_d = 1h$, $3h$, $9h$, $500h$. An independent sound source with constant amplitude of incident wave is assumed at the upstream.

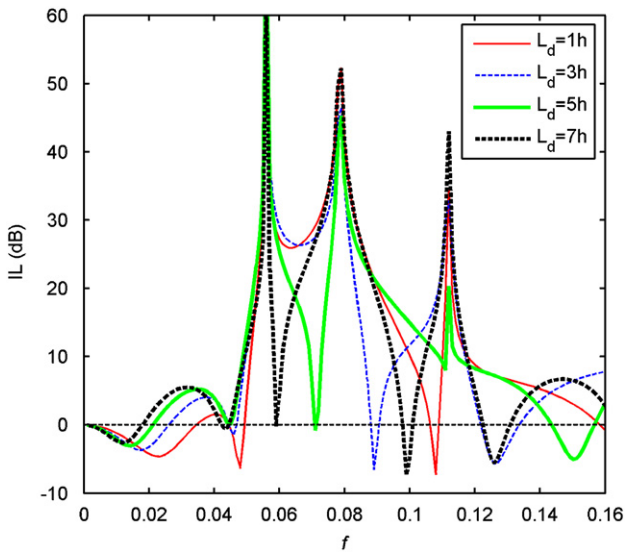

Fig. 5. Variation of IL spectra with respect to the distance from the expansion chamber exit to the downstream end, L_d, for a clamped plate silencer with $L = 5$, $h_c = 1$, $m = 2.4$ and $B = 0.11$. An independent sound source with constant amplitude of incident wave is assumed at the upstream.

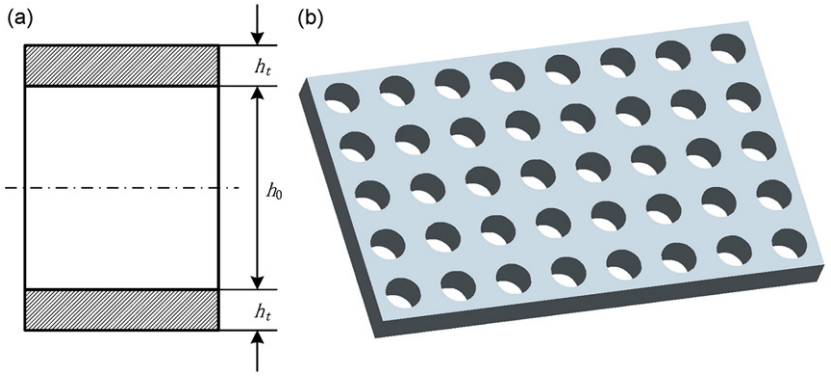

Fig. 6. Schematic representation of the sandwich construction. (a) Cross-sectional view of the sandwich plate which consists of two thin skin sheets each of thickness, h_t, and a thick core of thickness, h_0. (b) The perforated foam core used in the sandwich construction. Hole diameter: 5 mm.

The three terms on the right-hand side of the above expression represent, respectively, the bending of the skins about their centroidal axis, bending of the skins about the centroid of the whole beam, and bending of the core itself. The effect of shear deflection is negligible compared with the bending deflection; hence, it is neglected in calculating the flexural rigidity of the sandwich beams. Since the sandwich beam is treated as a homogeneous one, its equivalent Young's modulus is estimated as

$$E = B/I \tag{31}$$

with

$$I = \frac{(h_0 + 2h_t)^3}{12}. \tag{32}$$

According to the study by Huang [7], for a homogeneous plate of rectangular cross-section, the dimensionless bending stiffness is found to be

$$B = \frac{m^3 E}{12\rho_s}, \tag{33}$$

where m is the mass ratio, E is the dimensionless Young's modulus and ρ_s is the dimensionless density. Eq. (33) shows that, for a given set of m and B to be satisfied, the only crucial material property is $E/{\rho_s}^3$. An optimal design of the sandwich plate is the one that has the highest ratio of $E/{\rho_s}^3$, which is determined by the ratio between the thicknesses of the thin facing sheet, h_t, and the core, h_0. As shown in Fig. 7(a), $E/{\rho_s}^3$ varies as a function of h_t/h_0, and the maximum value, $E/{\rho_s}^3 = 0.1453$, is reached when $h_t/h_0 = 0.003$. Keeping h_t/h_0 at the optimal value of 0.003, Eq. (33) gives the achievable maximum bending stiffness, B_1, of the sandwich plate for a given mass ratio m. The feasibility of using the proposed sandwich beam to realize the low-frequency plate silencer is investigated below. Note that the optimal bending stiffness B_{opt} for a plate silencer to function with the widest bandwidth also varies with m. Fig. 7(b) compares the maximum bending stiffness of the sandwich plate, B_1 (solid line), with the required optimal bending stiffness B_{opt} (solid line with open circles) as functions of m. As shown in Fig. 7(b), the proposed sandwich plate design would satisfy the optimal bending stiffness condition when the mass ratio is around $m = 2$. In practice, a loss of bending stiffness may occur and the predicted bending stiffness for the sandwich construction cannot be fully reached as in the case reported in the following experimental study. Assuming that only 50% of the predicted bending stiffness can be obtained, the corresponding bending stiffness B_2 is shown in Fig. 7(b) in dashed line. In this case, a sandwich plate with mass ratio $m = 2.7$ would become stiff enough for the optimal design of the plate silencer.

For comparison purposes, three types of sandwich plates with different mechanical properties are manufactured by bonding two aluminium sheets of thickness 0.025 mm to different Rohacell® foam cores using epoxy resin. For the first type (designated as type I), the core thickness is 4 mm, and a series of holes

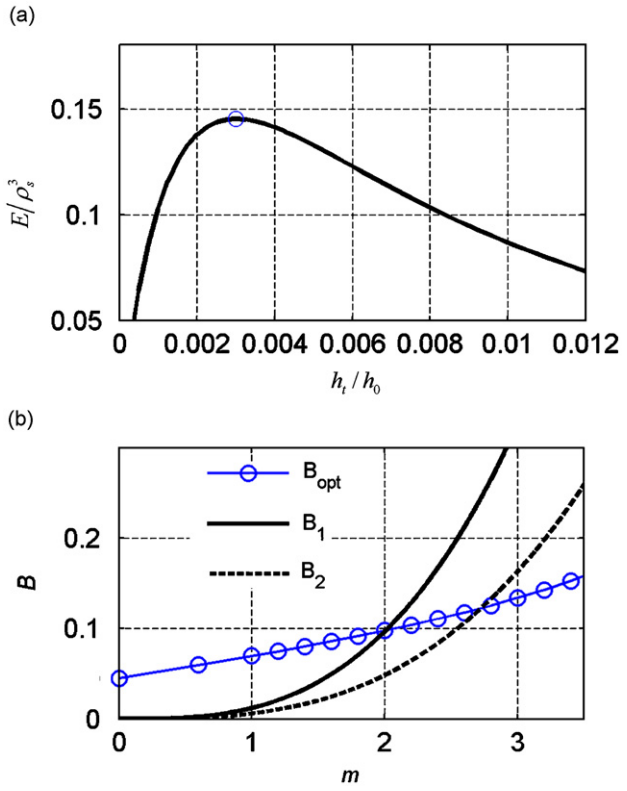

Fig. 7. Optimal design of the sandwich construction with given core material (Rohacell IG-31) and skin sheet (aluminium). (a) Variation of E/ρ_s^3 with respect to the ratio of h_t/h_0. (b) Comparison between the achievable maximum bending stiffness, B_1, and the required optimal bending stiffness B_{opt}. The curve for B_2 shows the situation where 50% loss of bending stiffness occurs during the sandwich construction.

Table 1
Properties of the sandwich plates

Type	Core thickness (mm)	Plate-to-air mass ratio, m	Equivalent dimensionless B	Perforation ratio of core
I	4	2.4	0.061	35%
II	4	2.75	0.061	n/a
III	3	2.4	0.037	n/a

(diameter: 5 mm) are drilled on the core with a perforation rate of about 35%, as shown in Fig. 6(b). The perforation can reduce the weight of the final sandwich plate while the bending stiffness remains nearly unchanged. For type II and III, the core thickness is 4 and 3 mm, respectively, without any perforation. The final surface density of the three sandwich plates are, 0.3, 0.337, and 0.3 kg/m^2, respectively. The equivalent Young's modulus E^* is measured through three-point bending test as, 1.61, 1.61, and 2.32 GPa. In the following experimental study, the cross-section of the rigid duct is of the size 100 mm × 100 mm. For the given duct size, the dimensionless bending stiffness and mass ratio for the three plates can be calculated using the normalization scheme described in Section 2, as listed in Table 1.

4. Experimental study

The performances of three plate silencers are studied experimentally. Depending on the types of the sandwich plate used, the three silencers are designated as silencer I, silencer II, and silencer III, respectively.

Since the sandwich plate type I has the best mechanical properties (the highest bending stiffness; the lowest mass ratio) out of the three sandwich constructions, it is expected to perform better than the other two.

4.1. Experimental rig

The test rig was built with a small square duct with a cross-section of 100 mm × 100 mm. The duct wall was made of 15-mm-thick acrylic, which can be considered as acoustically rigid. The two side-branch cavities also had a cross-section of 100 mm × 100 mm and the length was 500 mm. With the given geometry, the first cut-on frequency in the rigid duct is about 1700 Hz. Two pieces of sandwich plates of the same type were installed flush with the duct wall. For types I and II, the plates are of the size 518 mm × 102 mm × 4 mm. For type III, the plate is of the size 518 mm × 102 mm × 3 mm. The leading and trailing edges of the plates were clamped, and the final effective length of the plates was 500 mm. The two lateral edges of the plates were inserted into a thin gap between the two constituent plates of the cavity walls. The clearance between the lateral edges of the plates and the cavity walls is less than 0.5 mm. Such a configuration was adopted to make sure that the plates can vibrate freely in the y direction and minimize the leakage of noise from the main duct to the cavities via the gap. A four-microphone, two-load measurement system was adopted to measure the TL, sound energy reflection coefficients and absorption coefficients. Details of the measurement system can be found in Refs. [5,8] and are not repeated here.

4.2. Benchmark results for silencer I

The measured data for silencer I are shown in Fig. 8. The TL spectrum is shown in Fig. 8(a) in thin solid curve with open circles, together with the predicted performance of the expansion chamber of the same cavity geometry (dashed curve) for comparison. Three spectral peaks are observed in the measured TL curve of the plate silencer at frequencies: 140, 250, and 420 Hz. The first two peaks and the trough between them form a continuous frequency band within which good noise reduction level is obtained. With a criterion level $TL_{cr} = 10$ dB, a wide stopband, $f^* \in [133\,\text{Hz}, 273\,\text{Hz}]$, or in the dimensionless form, $f \in [0.039, 0.08]$, can be observed. The logarithmic bandwidth for silencer I is $f_2/f_1 = 2.1$, which is slightly larger than one octave. According to Huang [16], a dimensionless frequency of 0.077 can be chosen as a demarcation line for the

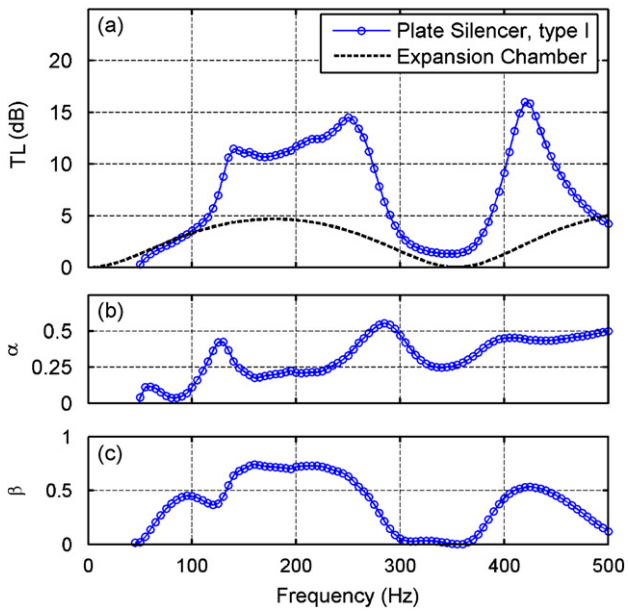

Fig. 8. Measured data for plate silencer I. (a) TL. The predicted TL for an expansion chamber of the same cavity geometry is also given for comparison. (b) Absorption coefficient. (c) Reflection coefficient.

'medium' frequency below which the porous duct lining may be considered ineffective. Following this specification of 'medium' frequency, the stopband for silencer I, $f \in [0.039, 0.08]$, falls almost completely into the low-frequency region. The silencing performance between the second and third peaks, say, from 275 to 400 Hz, is unsatisfactory with low TL level. It can be shown by simulation that this phenomenon is caused by insufficient bending stiffness of the plate. The TL level can be lifted, for example, to above the criterion level, TL_{cr}, by adopting a stiffer plate, and a wider stopband is then expected. However, the trade-off is that the whole stopband will shift to higher-frequency region if the plate-to-air mass ratio remains the same.

Fig. 8(b) and (c) shows the measured sound energy absorption coefficient and reflection coefficient, respectively. At the stopband where the plate silencer functions effectively, the reflection coefficient dominates with an overall level of around 0.7, while the absorption coefficient is at a level of around 0.2–0.25. It confirms that main mechanism of sound reduction in the plate silencer is reflection, which conforms to the theoretical assumption of the plate silencer design. As frequency increases, the absorption coefficient becomes significant, reaching a level of around 0.5 at the relative high frequency.

4.3. Comparison with theoretical predictions

A comparative study is conducted between the experimental results and the theoretical predictions, as shown in Fig. 9. The solid curves with open circles show the measured data of silencer I. The corresponding predicted data are calculated using the mechanical properties listed in Table 1. An ideal design of a plate silencer assumes that there is no energy dissipation in the system and the noise reduction is purely caused by sound reflection due to the plate vibration. This extreme situation is simulated by taking $\sigma_m = \sigma_s = 0$ in the theoretical model, and the predicted data are shown in solid curves. However, several energy dissipation mechanisms exist in the real experimental rig, for example, cavity damping, structural damping in the plate- and sound-induced vibration of the duct walls. It was argued by Wang et al. [8] that the main energy dissipation mechanism in the plate silencer is the structural damping and a Rayleigh damping model can be adopted to characterize the sound absorption in the rig roughly. When the plate damping is included in the theoretical model, the corresponding predicted results are shown in dashed curves. The damping ratio for the sandwich plate is measured as 0.09. The mass and stiffness damping coefficients used in the Rayleigh damping

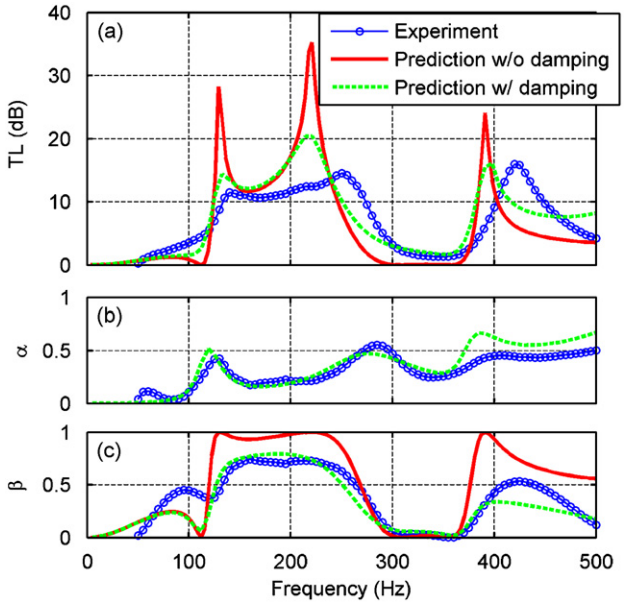

Fig. 9. Comparison of experimental data (solid curves with open circles) with theoretical predictions (solid curves: without structural damping; dashed curves: with structural damping) for plate silencer I. (a) TL. (b) Absorption coefficient. (c) Reflection coefficient. The dashed curves are calculated with the structural damping of the plate modelled as $\sigma_m = 0.15$ and $\sigma_s = 0.05$.

model are

$$\sigma_m = 0.15, \quad \sigma_s = 0.05, \tag{34}$$

which correspond to an equivalent damping ratio of 0.1. Considering that the plate damping is not the only damping mechanism in the experimental rig, the plate damping ratio used in the theoretical model is slightly larger than the measured value of 0.09.

Fig. 9(a) compares the predicted and measured TL spectra. When damping effects are excluded, the noise reduction is caused by sound reflection only and three sharp spectral peaks can be observed in the predicted TL spectrum (solid curve). The main effect of damping inside the experimental rig is to smooth out the TL peaks, as illustrated by the dashed curve which is predicted by adopting a Rayleigh damping model. The damping effect on the amplitude of the TL peaks (smoothing out) is quite significant. However, as the purpose is to achieve a wide stopband, the absolute values at the resonant peaks are of little concern as long as they are still above the criterion value, TL_{cr}. The existence of damping mechanism in the experimental rig also causes slight frequency shift of the TL peaks. When homogeneous plate is used, the frequency discrepancy between the predicted and measured TL peaks is negligible, as shown in Ref. [8] where balsawood plates were tested. However, the frequency shift is considerable in the present case, especially at the second and the third TL peaks where the measured TL peaks are shifted to higher frequencies, by 8% approximately. As the discrepancy is negligible in the case of homogeneous plate, it is reasonable to assume that the significant frequency shift is due to the modelling simplification of the sandwich construction in the current study. In this sense, a more advanced model that describes the coupling dynamics between the vibration of the sandwich plate and the acoustics would be necessary. Nevertheless, as the frequency of the measured TL peaks is always higher than the predicted ones by certain level, the frequency shift can be estimated in advance approximately.

Fig. 9(b) and (c) compares the sound absorption coefficient α and the sound reflection coefficient β, respectively. When the damping effects are excluded, there is no sound absorption in the prediction. Because of the existence of significant energy dissipation mechanism in the experimental rig, the level of the predicted reflection coefficient (solid curve) is higher than the measured one (solid curve with open circles).

When the plate damping is considered in the modelling, the predicted sound absorption coefficient and reflection coefficient (dashed curves) better agree with the measured ones (solid curves with open circles), especially in the low-frequency range. In summary, it is appropriate to predict the performance of a sandwich plate silencer using a simplified theoretical model based on homogeneous plate. The damping mechanism inside plate silencer can be roughly characterized by the structural damping of the sandwich plate.

4.4. Effect of mass ratio and bending stiffness

Silencer II and silencer III are also tested and their results are compared with silencer I to show the variation of silencing performance with different plate mass ratios and bending stiffnesses. Fig. 10(a) and (b) compares the measured and predicted TL spectra, respectively. The damping coefficients are chosen as $\sigma_m = 0.15$ and $\sigma_s = 0.05$ in the predictions for all the three silencers. The effect of plate mass is generally counterproductive, which is partly verified by the comparison between silencer I and silencer II. The two silencers have almost the same bending stiffness but different plate mass ratios. Since the mass ratio for silencer I ($m = 2.4$, $B = 0.061$) is smaller than silencer II ($m = 2.75$, $B = 0.061$), it has a wider bandwidth and higher TL level between the first two spectral peaks, as shown in both Fig. 10(a) and (b). Note that the spectral peaks and the whole stopband for silencer I shift a little towards higher frequency. However, it does not necessarily mean that a heavier plate can achieve better low-frequency performance, since it has a lower trough between the first and second peaks. The performance comparison between silencer I ($m = 2.4$, $B = 0.061$) and silencer III ($m = 2.4$, $B = 0.037$) shows the importance of bending stiffness in the design of plate silencer. Due to the insufficient bending stiffness, the overall performance of silencer III drops significantly in comparison with silencer I, as shown in Fig. 10(a). The variation of the measured TL spectra between silencer I and silencer III conforms to the prediction shown in Figs. 10(b) and 3.

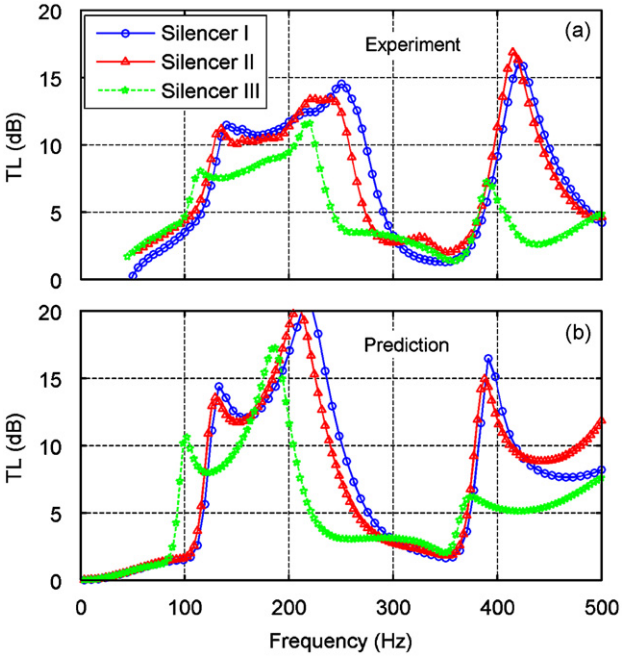

Fig. 10. TL comparison among three plate silencers with different plate properties (I: $m = 2.4$, $B = 0.061$; II: $m = 2.75$, $B = 0.061$; III: $m = 2.4$, $B = 0.037$). (a) Experimental results. (b) Predictions with the structural damping of the plate modelled as $\sigma_m = 0.15$ and $\sigma_s = 0.05$.

5. Concluding remarks

A broadband low-frequency plate silencer is experimentally realized using sandwich plate. The prototype plate silencer demonstrates much better silencing performance than the expansion chamber of the same geometry (expansion ratio = 3), with the stopband being from 133 to 274 Hz in which the TL is larger than a criterion value 10 dB over the whole frequency band. The performances of the sandwich plate silencers are predicted using a mathematical model based on homogeneous plate. As far as low frequency is concerned, the experimental results are in fair agreement with the predictions. Sandwich plates with different mechanical properties are also tested and compared, which partially confirms the theoretical findings on the effect of plate properties on the silencer performance.

Acknowledgments

The first author thanks the Hong Kong Polytechnic University for the Ph.D. studentship. The authors also would like to thank Dr. Y.S. Choy for providing some useful information in the IL calculation.

References

[1] F.P. Mechel, I.L. Vér, Sound-absorbing materials and sound absorbers, in: L.L. Beranek, I.L. Vér (Eds.), *Noise and Vibration Control Engineering, Principles and Applications*, Wiley, New York, 1992.
[2] K.U. Ingard, *Notes on the Sound Absorption Technology, Noise Control Foundation*, Poughkeepsie, New York, 1994.
[3] M.L. Munjal, S. Krishnan, M.M. Reddy, Flow-acoustic performance of perforated element mufflers with application to design, *Noise Control Engineering Journal* 40 (1993) 159–167.
[4] L. Huang, Modal analysis of a drumlike silencer, *Journal of the Acoustical Society of America* 112 (2002) 2014–2025.
[5] Y.S. Choy, L. Huang, Experimental studies of a drumlike silencer, *Journal of the Acoustical Society of America* 112 (2002) 2026–2035.
[6] Y.S. Choy, L. Huang, Effect of flow on the drumlike silencer, *Journal of the Acoustical Society of America* 118 (2005) 3077–3085.

[7] L. Huang, Broadband sound reflection by plates covering side-branch cavities in a duct, *Journal of the Acoustical Society of America* 119 (2006) 2628–2638.
[8] C. Wang, J. Han, L. Huang, Optimization of a clamped plate silencer, *Journal of the Acoustical Society of America* 121 (2007) 949–960.
[9] M.F. Ashby, *Material Selection in Mechanical Design*, second ed., Butterworth Heinemann, Oxford, 1999.
[10] F.J. Plantema, *Sandwich Construction, the Bending and Buckling of Sandwich Beams, Plates, and Shells*, Wiley, New York, 1966.
[11] E. Nilsson, A.C. Nilsson, Prediction and measurement of some dynamic properties of sandwich structures with honeycomb and foam cores, *Journal of Sound and Vibration* 251 (2002) 409–430.
[12] D.J. Inman, *Engineering Vibration*, Prentice-Hall, Englewood Cliffs, New Jersey, 2001.
[13] P.E. Doak, Excitation, transmission and radiation of sound from source distributions in hard-walled ducts of finite length, (I): the effects of duct cross-section geometry and source distribution space-time pattern, *Journal of Sound and Vibration* 31 (1973) 1–72.
[14] H. Kuttruff, *Room Acoustics*, E & FN Spon, New York, 2000.
[15] L. Huang, Y.S. Choy, Vibroacoustics of three-dimensional drum silencer, *Journal of the Acoustical Society of America* 118 (2005) 2313–2320.
[16] L. Huang, Parametric studies of a drumlike silencer, *Journal of Sound and Vibration* 269 (2004) 467–488.
[17] M.L. Munjal, *Acoustics of Ducts and Mufflers with Application to Exhaust and Ventilation System Design*, Wiley-Interscience, New York, 1987.
[18] Y.S. Choy, L. Huang, Drum silencer optimized for NC-weighted insertion loss, *Proceedings of Noise-Conference October 2007*, Reno, Nevada.
[19] A.D. Pierce, *Acoustics: An Introduction to its Physical Principles and Applications*, fourth ed., Acoustical Society of America, New York, 1989.
[20] ROHACELL, *Technical Manual*, Darmstadt: Röhm GmbH, Germany, 1987.
[21] H.G. Allen, *Analysis and Design of Structural Sandwich Panels*, Pergamon Press, Oxford, 1969.